Quantitative Analysis of Nonequilibrium Spin Injection into Molecular Tunnel Junctions

Zhanyu Ning,[1] Yu Zhu,[1] Jian Wang,[2] and Hong Guo[1]

[1]*Centre for the Physics of Materials and Department of Physics, McGill University, Montreal, QC, Canada H3A 2T8*

[2]*Department of Physics, The University of Hong Kong, Pokfulam Road, Hong Kong, China*

(Received 23 October 2007; published 6 February 2008)

We report quantitative analysis of nonequilibrium spin injection from Ni contacts to the octanethiol molecular spintronic system. Our calculation is based on carrying out density functional theory within the Keldysh nonequilibrium Green's function formalism. The first principles results allow us to establish a clear physical picture on how spins are injected from the Ni contacts through the Ni-molecule linkage to the molecule, why tunnel magnetoresistance is rapidly reduced by the applied bias in an asymmetric manner, and to what extent *ab initio* transport theory can make quantitative comparisons to the corresponding experimental data. We found that extremely careful sampling of the two-dimensional Brillouin zone of the Ni surface is crucial for accurate results.

DOI: 10.1103/PhysRevLett.100.056803 PACS numbers: 85.65.+h, 72.25.−b, 85.35.−p, 85.75.−d

Using molecules as *spin* transport elements has led to the notion of molecular spintronics [1] which has attracted considerable attention both experimentally [2–9] and theoretically [10–16]. Molecular spintronics exploits chemistry for control and manipulating quantum transport of spin—in addition to charge, down to the single molecule level: a perspective that has not existed before. Molecular spintronics is only at its infancy and requires careful and *quantitative* investigations to establish a physical picture on many important and general issues. These include, what controls spin injection from ferromagnetic contacts to the molecule, what role is played by external bias voltage, how spin transport is related to chemical details and to what extent state-of-the-art theory can compare with measured data.

To address these important problems, we have focused on the experimental device of Ref. [5] which reports low temperature quantum spin transport in octanethiol molecules connected to the outside world by Ni contacts using nanopores [17]. The data [5] showed that the tunnel magnetoresistance ratio (TMR) of this device is asymmetric with respect to the polarity of bias voltage V_b, the TMR decays from its peak value to zero when V_b is greater than several tens of millivolts, and the largest peak TMR is about 16%. This experiment has inspired many theoretical works on molecular spintronics [11–16] at a *qualitative* level. However, there has been no *quantitative* comparison and understanding between first principles analysis and the experimental data. Our calculation is based on a state-of-the-art first principles method where real space density functional theory (DFT) is carried out within the nonequilibrium Green's function (NEGF) framework [15,18]. The basic idea of NEGF-DFT formalism is to calculate the device Hamiltonian and electronic structure by DFT, deal with the nonequilibrium quantum transport condition by NEGF, and account for the open device boundary conditions by real space numerical procedures. We refer interested readers to Refs. [15,18] for details of the NEGF-DFT formalism.

The device we consider consists of two semi-infinite Ni(100) slabs sandwiching 8-octanethiols, $C_8H_{17}S$, shown in the inset of Fig. 1. The Ni slabs extend to $z = \pm\infty$ along the transport direction z. The system extends periodically in the transverse x, y directions with a unit cell whose cross section is 3.52×3.52 Å^2. We divide the Ni-octanethiol-Ni device into a scattering region consisting of the molecule and four layers of Ni atoms on either side, and left or right Ni leads. The atomic structure of the scattering region is relaxed using the total energy DFT electronic package SIESTA [19], where the outmost layers of Ni atoms are fixed at their bulk positions. In NEGF-DFT calculations, we adopt double zeta-polarized basis for C, H, and S, and single zeta-polarized basis for Ni atoms. The exchange-correlation is treated at the local spin density approximation level. As a check, we verified that the calculated band structure, density of states (DOS,) and spin splitting for bulk Ni are in excellent agreement with known results [20].

A major difficulty in calculating transport of Ni-octanethiol-Ni is the enormous number of k points neces-

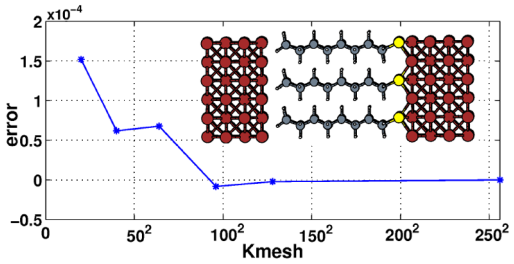

FIG. 1 (color online). Convergence of Green's function with respect to size of k mesh. Verticle axis: Error $\equiv \mathrm{Tr}(|G^r|)/\mathrm{Tr}(|G^r(256^2k\text{-mesh})|) - 1$. For 96×96 or greater k mesh, the result is converged. See Ref. [22] for more discussion. Inset: schematic of the device which has an asymmetric atomic structure.

sary for sampling the two-dimensional (2D) Brillouin zone (BZ). In the NEGF-DFT analysis [15,18], the nonequilibrium density matrix is calculated by NEGF, $\hat{\rho} = \int_{\mathrm{BZ}} dk_{\|} \hat{\rho}_{k_{\|}}$ with $\hat{\rho}_{k_{\|}} \sim \int dE \mathbf{G}^{<}_{k_{\|}}(E)$. Here $k_{\|} \equiv (k_x, k_y)$ samples the 2D BZ of the Ni leads. The NEGF $G^{<}_{k_{\|}} = G^{r}_{k_{\|}} \Sigma^{<}_{k_{\|}} G^{a}_{k_{\|}}$ where $G^{a}_{k_{\|}} = (G^{r}_{k_{\|}})^{\dagger}$ is the advanced Green's function, and $\Sigma^{<}_{k_{\|}}$ is the lesser self-energy given by a linear combination of the Fermi-Dirac functions of the two leads [21], $\Sigma^{<}_{k_{\|}} = i\Gamma_{L,k_{\|}} f_L + i\Gamma_{R,k_{\|}} f_R$, where the line-width functions of left or right leads $\Gamma_{L,R}$ describe coupling of the scattering region to the leads, and can be calculated by standard methods [18]. All quantities are calculated for each $k_{\|}$ and summed over the 2D BZ. For our problem, the fine electronic structures in the BZ of the Ni surface and the sharp transmission resonances require very careful examination of the k sampling. Since it is unclear how to reduce the k points due to the lack of symmetry, we apply an adaptive sampling technique with a very fine k mesh. To find out how fine it should be, we calculated the retarded Green's function $G^{r}_{k_{\|}}$ with an enormous k mesh of 256×256 k points and use this as a benchmark. We then reduce the k-mesh: the difference of $|G^{r}_{k_{\|}}|$ for smaller k mesh and the benchmark is shown in Fig. 1. It shows that a k mesh of at least 96×96 is necessary to converge the BZ integration of the density matrix $\hat{\rho}$. A smaller mesh does not give sufficiently accurate results [22]. Therefore we fix the k mesh to be 96×96 in all our calculations, which means that for each iteration step toward self-consistency, 96^2 independent NEGF-DFT calculations must be performed for each energy E (up to 110 E points) to converge the density matrix, and this is repeated for each bias voltage. After the self-consistent NEGF-DFT procedure is converged, we calculate total transmission coefficient for spin channel σ by a second BZ integration using the same k mesh,

$$T_{\sigma}(E) = \int_{-\pi}^{\pi} \frac{dk_{\|}}{(2\pi)^2} \tilde{T}_{\sigma}(E, k_{\|}), \tag{1}$$

where $\tilde{T}_{\sigma}(E, k_{\|})$ is the BZ-resolved transmission function for a given $k_{\|}$. It is obtained by [15]

$$\tilde{T}_{\sigma}(E, k_{\|}) = \mathrm{Tr}[G^{r}_{k_{\|}} \Gamma_{L,k_{\|}} G^{a}_{k_{\|}} \Gamma_{R,k_{\|}}], \tag{2}$$

where all quantities on the right hand side are functions of energy E.

Figures 2(a)–2(d) plot quantity $\tilde{T}_{\sigma}(E, k_{\|})$ at zero bias versus $k_{\|} = (k_x, k_y)$ when magnetic moments of the Ni leads are in parallel or antiparallel configurations (PC or APC). These are obtained at the Fermi energy of the Ni leads (shifted to $E_F = 0$). The main impression is the "hot spots" in the BZ where $\tilde{T}_{\sigma}(E, k_{\|})$ has very sharp resonance features at various points of $k_{\|}$, indicated by high values of $\tilde{T}_{\sigma}$ (hot color) on top of a rather smooth background value (cold color). Hot spots are known to exist in conventional

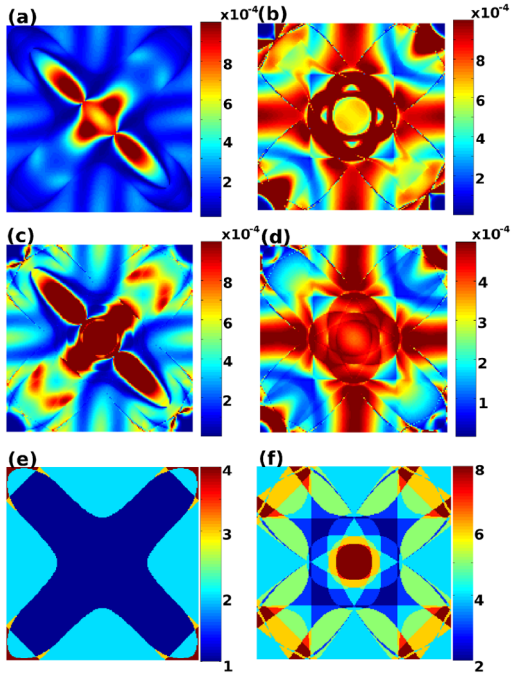

FIG. 2 (color online). (a)–(d) Zero bias transmission coefficient at E_F in the 2D Brillouin zone. (a) Spin-up channel for PC; (b) spin-down for PC; (c) spin-up for APC; (d) spin-down for APC. Note the different transmission scales indicated by the vertical bar. (e) and (f) Number of incoming channels in the Ni-lead at E_F in 2D BZ. Note spin-up electron is majority carrier but has less DOS at E_F. For this reason the number of conducting channel of spin-up, (e), is less than that of spin-down, (f).

magnetic tunnel junctions [23]. For the molecular junction here, we find that the smooth background of $\tilde{T}_{\sigma}(E, k_{\|})$ is largely due to transmission channels in the Ni leads that tunnel through the molecular layer, while the hot spots are due to resonance transmission which is sensitive to $k_{\|}$. To understand the smooth background (cold color regions) of $\tilde{T}_{\sigma}(E, k_{\|})$, Fig. 2(e) and 2(f) plot the BZ-resolved number of conducting channels in the Ni lead at E_F: the spin-up channel is of a 4-petal pattern with channel number 1 to 4; the spin-down channel is a complicated pattern with channel number 2 to 8. The symmetry of the transmission pattern is due to the fact that the CH2 groups of alkanethiols are roughly oriented along one of the diagonals of the Ni-(100) unit-cell. These patterns are rather similar to the cold color regions of Fig. 2(a) and 2(b) for PC. For APC, Fig. 2(c) and 2(d) are a combination of both spin-up and -down channel patterns as expected. To understand the sharp hot spot features, we calculated real space scattering wave functions at various $k_{\|}$. When $k_{\|}$ is not on a hot spot, the modular of the wave function essentially decays exponentially along the molecule; but when $k_{\|}$ is on a hot spot, the wave function oscillates indicating resonance.

The chemical properties are found to substantially affect spin transport and determine how spins are injected. The main contribution to the DOS of bulk Ni at E_F is due to the

spin-polarized d waves. An octanethiol is composed of CH_2 units connected by σ-bonds which are sp_3 hybridized orbitals. Therefore, the p wave is more likely to propagate along the linear chain. For analysis purposes, we may consider that the interfaces between molecules and leads serve to connect d to p waves. Quantitatively, we define a spin resolved *partial transmission* from Eq. (2), $P_{AB} \equiv \sum_{A,B} G^r_{b_1 a_1}(\Gamma_L)_{a_1 a_2} G^a_{a_2 b_2}(\Gamma_R)_{b_2 b_1}$, where A and B are wave labels of s, p, d_1, d_2, here $d_1 = d_{xy}$, d_{yz}, d_{xz} and $d_2 = d_{x^2-y^2}$, $d_{r^2-3z^2}$. $a_{1,2} \in A$ are orbital indices for the left lead with label A; $b_{1,2} \in B$ are for right lead with label B. The quantity P_{AB} measures the probability of an A-type wave in the left lead propagating to a B-type wave in the right traversing the molecule. Table I shows P_{AB} computed at the Γ-point where data larger than 30% of the maximum are highlighted in boldface. In PC, spin-up electrons are actually the minority carriers at E_F for Ni, their P_{AB} values are distributed into all types of orbitals, see upper-left block of the table. In clear contrast, the spin-down channel is dominated by the d wave to d wave transmission, shown in lower-left block, corresponding to tunneling processes of majority d waves. In APC, spin-up electrons are minority carriers for the left lead and majority carrier for the right. The contribution to the spin-up transport channel comes from all different waves in the left lead scattered into d waves of the right lead, shown in upper-right block. The spin-down channel is given by majority (left) to minority (right) scattering, hence we observe d waves from left scattering into all the other waves of the right (see lower-right block). These scattering processes suggest that spin injection can be tuned and controlled chemically through the molecules in the middle.

TABLE I. Values of partial transmission P_{AB} at Γ-point from left to right lead. First column indicates partial wave labels of the left lead (incoming), the first row is for right lead (outgoing). Arrows indicate spin channels. Some values are much larger than others, indicating those scattering channels are dominating. Data larger than 30% of the maximum are highlighted in boldface.

	Parallel (10^{-5})					Antiparallel (10^{-5})			
$L\}R(\uparrow)$	s	p	d_1	d_2	$L\}R(\uparrow)$	s	p	d_1	d_2
s	**89**	**42**	**58**	**37**	s	50	24	**309**	**208**
p	**43**	25	**30**	17	p	24	14	**163**	**121**
d_1	**65**	**32**	**84**	**32**	d_1	38	16	**288**	**203**
d_2	**38**	17	**29**	19	d_2	17	8	**126**	81
$L\}R(\downarrow)$	s	p	d_1	d_2	$L\}R(\downarrow)$	s	p	d_1	d_2
s	16	50	84	43	s	20	8	20	8
p	6	5	40	29	p	10	6	10	5
d_1	145	65	103	**663**	d_1	**233**	**177**	**268**	**116**
d_2	61	42	**558**	**544**	d_2	**141**	**94**	**143**	**72**

Using Eq. (1) we obtain spin-polarized current

$$I_\sigma(V_b) = \frac{e}{h} \int_{\mu_L}^{\mu_R} T_\sigma(E, V_b)(f_L - f_R) dE, \qquad (3)$$

where $\mu_{L,R}$ are electrochemical potentials of the left or right leads and $\mu_L - \mu_R = eV_b$, and $f_{L,R} \equiv f(E - \mu_{L,R})$ are the Fermi functions. The total charge current is given by $\sum_\sigma I_\sigma$. Figure 3 shows the I-V curve for PC and APC as well as TMR defined by the total currents, TMR $= (I_{\rm PC} - I_{\rm APC})/I_{\rm APC}$. At $V_b = 0$ we compute TMR by the equilibrium transmission coefficient.

For our device, $I_{\rm PC} > I_{\rm APC}$ for the entire bias range -200 mV $< V_b < +120$ mV we examined, giving rise to positive TMR versus V_b. TMR is asymmetric with respect to the polarity of V_b, in agreement with the experiment [5]. This asymmetry is due to the asymmetric atomic structure: only one side of the molecule has the thiol group. In fact, the effect of asymmetry is already seen in Fig. 2(c) and 2(d): if the system were symmetric, then for APC at zero bias, the spin-up and -down channels would have exactly the same transmission. The fact that Figs. 2(c) and 2(d) are very different is an indiction of lack of symmetry. Quantitatively, we obtain a maximum TMR of 33% at $V_b = -20$ mV. The experimental data shows a maximum TMR about 12% to 16%, at -15 mV to -5 mV [Fig. 4(c) of Ref. [5]]. The calculated TMR decays as a function of V_b asymmetrically: it vanishes at $V_b < -200$ mV or at $V_b > +120$ mV (see Fig. 3). Experimentally [5], TMR also decays with bias asymmetrically but with voltage scales that are somewhat smaller than our theoretical values.

To understand why TMR decays with bias, we plot total transmission $T(E) = \sum_\sigma T_\sigma(E)$ versus energy E at four different values of V_b in Fig. 4. The vertical lines indicate the bias window, i.e., integration range of Eq. (3). For small V_b, $T(E)$ for PC and APC are rather different in the bias window, see Fig. 4(a) and 4(b). As $|V_b|$ is increased to larger values, the difference is reduced as shown in Fig. 4(c) and 4(d). Such a reduction is related to the DOS of Ni leads, it causes TMR to reduce with V_b. It is well known that there is a sharp peak in minority DOS (spin-

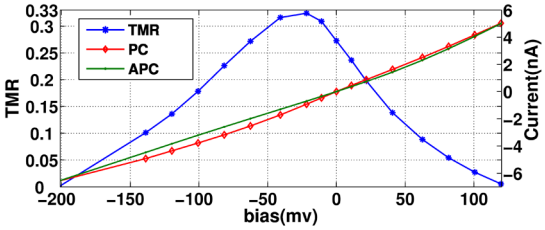

FIG. 3 (color online). I-V curves (right axis, per molecule) and voltage dependence of TMR (left axis). The solid line with diamond (red) and solid-dot (green) are I-V curves for PC and APC. The TMR-V curve (blue line with solid-star) peaks at -20 mV with 33% and decays to zero at -200 mV and $+120$ mV.

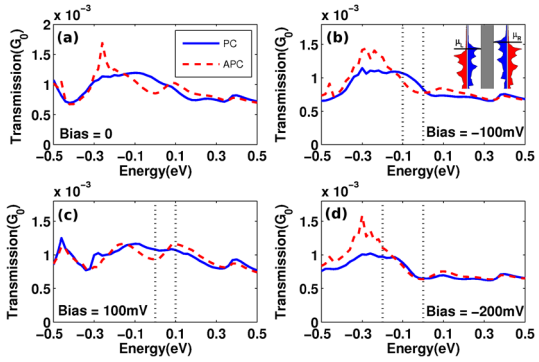

FIG. 4 (color online). The four panels are total transmission $T(E)$ versus energy E for PC (solid blue line) and APC (dashed red line) for four different V_b. The difference of PC and APC transmission within the energy window (marked by two dotted vertical lines) reduces for increasing $|V_b|$. Inset in (b): DOS of the Ni leads.

down) near the E_F of Ni, see inset of Fig. 4(b). At low bias, this DOS peak of left or right leads aligns, leading to a larger total transmission for PC than for APC, hence a larger TMR. As $|V_b|$ is increased, these DOS peaks are shifted away from each other so that the difference of transmission in PC and APC is reduced. $T(E)$ in the bias window has a major difference in terms of polarity of V_b. Namely, at $V_b = +100$ mV the PC and APC difference is already very small; but at $V_b = -100$ mV this difference is still substantial. This gives the asymmetrical TMR versus V_b. As discussed above, the asymmetry versus V_b is due to asymmetry of the atomic structure. Our calculation reveals that due to proximity effect, the S atom develops a small magnetic moment of a few percent Bohr magneton. This induced moment of S has a bias dependence similar to that of the TMR curve in Fig. 3 and clearly affects spin transport.

In summary, we have provided a direct and quantitative comparison on spin injection in molecular spintronics with the corresponding experimental data. We show that, to obtain accurate results, enormous k sampling is necessary. In this sense, our results provide a benchmark for further theoretical calculations. While we focused on discussing Ni-octanethiol-Ni which were measured experimentally, we have also performed similar calculations for Ni-hexanethiol-Ni and obtained qualitatively comparable results. Transport properties of molecular spintronics depends on chemical details of the molecule with high sensitivity, in our case, on how d waves from a Ni lead are scattered into p waves of the molecule before exiting to the second Ni lead. At the present stage of molecular spintronics researches, the quantitative consistency in many aspects with the measured data is rather satisfactory and provides a starting point to resolve the remaining differences.

We thank Dr. D. Waldron for participation at the early stage of this work and help on the NEGF-DFT package. This work is supported by NSERC of Canada, FQRNT of Quebec and CIAR (H. G.), and a RGC Grant (No. HKU 7048/06P) from the government SAR of Hong Kong (J. W.). We are grateful to RQCHP for providing the computation facility.

[1] S. A. Wolf *et al.*, Science **294**, 1488 (2001).
[2] K. Tsukagoshi, B. W. Alphenaar, and H. Ago, Nature (London) **401**, 572 (1999).
[3] V. Dediu *et al.*, Solid State Commun. **122**, 181 (2002).
[4] M. Ouyang and D. D. Awschalom, Science **301**, 1074 (2003).
[5] J. R. Petta, S. K. Slater, and D. C. Ralph, Phys. Rev. Lett. **93**, 136601 (2004).
[6] Z. H. Xiong, D. Wu, Z. V. Vardeny, and J. Shi, Nature (London) **427**, 821 (2004).
[7] T. X. Wang *et al.*, Appl. Phys. Lett. **88**, 242505 (2006).
[8] W. Harneit *et al.*, Phys. Rev. Lett. **98**, 216601 (2007).
[9] S. Pramanik *et al.*, Nature Nanotechnology **2**, 216 (2007).
[10] H. Mehrez, J. Taylor, Hong Guo, J. Wang, and C. Roland, Phys. Rev. Lett. **84**, 2682 (2000).
[11] R. Pati, L. Senapati, P. M. Ajayan, and S. K. Nayak, Phys. Rev. B **68**, 100407(R) (2003); L. Senapati, R. Pati, and S. C. Erwin, Phys. Rev. B **76**, 024438 (2007).
[12] E. G. Emberly and G. Kirczenow, Chem. Phys. **281**, 311 (2002); H. Dalgleish and G. Kirczenow, Phys. Rev. B **72**, 184407 (2005); **73**, 235436 (2006).
[13] R. Liu, S. H. Ke, H. U. Baranger, and W. T. Yang, Nano Lett. **5**, 1959 (2005).
[14] A. R. Rocha *et al.*, Nat. Mater. **4**, 335 (2005).
[15] D. Waldron *et al.*, Phys. Rev. Lett. **96**, 166804 (2006); D. Waldron, L. Liu, and H. Guo, *Molecular and Biological Devices*, a Special Issue of Nanotechnology **18**, 424026 (2007).
[16] B. Wang, Y. Zhu, W. Ren, J. Wang, and H. Guo, Phys. Rev. B **75**, 235415 (2007).
[17] W. Wang, T. Lee, and M. A. Reed, Phys. Rev. B **68**, 035416 (2003).
[18] J. Taylor, H. Guo, and J. Wang, Phys. Rev. B **63**, 245407 (2001); **63**, 121104 (2001).
[19] J. Junquera, O. Paz, D. Sanchez-Portal, and E. Artacho, Phys. Rev. B **64**, 235111 (2001).
[20] http://cst-www.nrl.navy.mil/ElectronicStructureDatabase/.
[21] S. Datta, *Electronic Transport in Mesocopic System* (Cambridge University Press, Cambridge, England, 1997).
[22] In Fig. 1 the difference of $|G^r|$ by smaller k mesh to the benchmark is $\sim 10^{-4}$. Although this appears to be small, it translates to larger error in density matrix to influence quantitative transport results. The reason is that error due to small k mesh is not uniformly distributed in matrix elements of G^r.
[23] O. Wunnicke *et al.*, Phys. Rev. B **65**, 064425 (2002).